First-order event plane correlated directed and triangular flow from fixed-target energies at RHIC-STAR

Sharang Rav Sharma (for STAR Collaboration)

Indian Institute of Science Education and Research (IISER) Tirupati

November 30, 2023

Abstract

We report the measurement of first-order event plane correlated directed flow (v_1) and triangular flow v_3 for identified hadrons ($\pi^\pm$, $K^\pm$, and p), net-particle (net-K, net-p), and light nuclei (d and t) in Au+Au collisions at $\sqrt{s_{\mathrm{NN}}} = 3.2$, 3.5, and 3.9 GeV in fixed-target mode from the second phase of beam energy scan (BES-II) program at RHIC-STAR. The v_1 slopes at mid-rapidity for identified hadrons and net-particles except π^+ are found to be positive, implying the effect of dominant repulsive baryonic interactions and spectator shadowing. The slope of v_1 for net-kaon undergoes a sign change from negative to positive at a lower collision energy compared to net-proton. An approximate atomic mass number scaling is observed in the measured v_1 slopes of light nuclei at mid-rapidity, which favours the nucleon coalescence mechanism for the production of light nuclei. The v_3 slope for all particles decreases in magnitude with increasing collision energy, suggesting a notable integrated impact of the mean-field, baryon stopping, and collision geometry at lower collision energies.

1

1   Introduction

The primary objective of ultra-relativistic heavy-ion collisions at the Relativistic Heavy Ion Collider (RHIC) and the Large Hadron Collider (LHC) is to create and characterize a novel state of matter with partonic degrees of freedom, known as the Quark-Gluon Plasma (QGP). This state of strongly interacting matter is hypothesized to have been present during the initial microseconds following the Big Bang, and gaining an understanding of its properties holds the potential to offer insights into the evolution of the universe [1]. The lattice Quantum Chromodynamics (QCD) predicts a crossover region between the hadron gas and Quark-Gluon Plasma (QGP) around T=154 MeV at low μ_B [3]. At lower temperatures and higher μ_B, QCD-based models suggest a first-order phase transition concluding at a conjectured QCD critical point [4]. Numerous experimental observables measured at RHIC and LHC have presented compelling evidence of Quark-Gluon Plasma (QGP) formation for matter near $\mu_B = 0$. However, experimental confirmation of the existence of a critical point and a first-order phase transition at higher μ_B is still pending. Many signatures of QGP formation and associated characteristics of the medium have been proposed. This proceeding will briefly explore one of the proposed signatures, namely, anisotropic flow. The patterns of azimuthal anisotropy in particle production are commonly referred to as flow. In heavy-ion collisions, it can be obtained by studying the Fourier expansion of the azimuthal angle (ϕ) distribution of produced particles with respect to the reaction plane angle (ψ_R). The reaction plane is defined as the plane subtended by the impact parameter vector and the beam axis.

The particle azimuthal angle distribution is written in the form of a Fourier series [4],

$$E\frac{\mathrm{d}^3N}{\mathrm{d}p^3} = \frac{\mathrm{d}^2N}{2\pi p_T \mathrm{d}p_T \mathrm{d}y} \left\{ 1 + \sum_{n\geq 1} 2\,v_n \cos\left[n\left(\phi - \Psi_n\right)\right] \right\}, \tag{1}$$

where p_T, y, ϕ, and Ψ_n are particle transverse momentum, rapidity, azimuthal angle of the particle and the nth order event plane angle, respectively. The various (order n) coefficients in this expansion are defined as:

$$v_n = \langle \cos[n(\phi - \Psi_R)] \rangle \tag{2}$$

The angular brackets in the definition denote an average over many particles and events [4]. These flow anisotropy parameters offer an insight into collective hydrodynamic expansion and transport properties of the produced medium at higher collision energies, while they are sensitive to the compressibility of the nuclear matter and nuclear equation of state at lower collision energies. The first three Fourier expansion coefficients v_1 (directed flow), v_2 (elliptic flow) and v_3 (triangular flow) are sensitive probes for studying the properties

of the matter created in high-energy nuclear collisions.

At higher energies (nucleon-nucleon center-of-mass energy $\sqrt{s_{NN}} \gtrsim 27$ GeV), where the transit time of colliding nuclei $2R/\gamma\beta$ is smaller than the typical production time of particles [5], flow harmonics are predominantly influenced by the collective expansion of the initial partonic density distribution [6]. Conversely, at lower energies, the shadowing effect caused by passing spectator nucleons becomes significant. For $\sqrt{s_{NN}} \lesssim 4$ GeV, nuclear mean-field effects contribute to the observed azimuthal anisotropies [7]. Numerous studies indicate that flow coefficients are notably sensitive to the incompressibility of nuclear matter (κ) in the high baryon density region [8]. Comparing experimental data with results from theoretical transport models can provide constraints on κ, offering valuable insights into nuclear Equation of State (EOS).

The v_1, sensitive to early collision dynamics, is proposed as a signature of first-order phase transition based on a hydrodynamic calculation. These calculations, whose equation of state incorporates a first-order phase transition from hadronic matter to QGP, predict a non-monotonic variation of the slope of the directed flow of baryons (and net-baryons) around midrapidity as a function of beam energy [9].

The tradional v_3, third order flow coefficient typically results from fluctuations in shape of the initial condition and is therefore not correlated to the reaction plane. Contrary to this, an observation has been made by the HADES collaboration at $\sqrt{s_{NN}} = 2.4$ GeV Au+Au collisions regarding a noticeable triangular flow, correlated with the first order event plane (Ψ_1) [6]. v_3 is also observed to be sensitive to the equation of state and can serve as a new tool to explore the time dependence of the pressure during the heavy-ion collision [10]. The evolution of v_3 is influenced by two crucial factors: the first involves the appropriate geometry determined by stopping, the passing time of spectators, and the expansion of the fireball; the second entails a potential within a responsive medium that propels the collective motion of particles.

2   Dataset and Event Selection Cuts

In these proceedings, we present the results of first order event plane (Ψ_1) correlated v_1 and v_3 for identified hadrons ($\pi^{\pm}$, $K^{\pm}$, and p), net-particle (net-K, net-p), and light nuclei (d and t) in Au+Au collisions at $\sqrt{s_{NN}} = 3.2$, 3.5, and 3.9 GeV using the fixed target (FXT) data from the Solenoidal Tracker at RHIC (STAR) experiment. The FXT setup was implemented at STAR to explore the region of high baryon chemical potential (μ_B) on the QCD phase diagram. This data was collected during the second phase of the Beam Energy Scan program (BES-II) (2019-2020) after incorporating various detector upgrades.

In FXT mode, where the target is stationary at one end of the TPC, we apply a vertex cut along the z-direction (v_z) within [198, 202] cm. For the x and y directions, we set the V_r ($\sqrt{V_x^2 + V_y^2}$) less than 2 cm centered around (0, -2).

3 Analysis Details

3.1 Track Quality Cuts

To ensure the quality of primary tracks, tracks with the transverse momentum p < 0.2 GeV/c are excluded. Additionally, we mandate the utilization of a minimum of 15 fit points and 52% of the total possible fit points in the track fitting process. The selection criterion involves choosing dE/dx hit points $\geq$ 10. Furthermore, the distance of closest approach (DCA) is set to < 3 cm.

3.2 Particle Identification

The identification of charged particles in STAR is done by the combination of Time Projection Chamber (TPC) and Time of Flight (TOF) detectors. For low-momentum particles, TPC is used, whereas for particles with intermediate or high momenta (p_T >1 GeV/c), the TOF is used. TPC uses the ionization energy loss (dE/dx) of the charged particles passing through it for particle identification. Using dE/dx information, the z variable is defined:

$$z = ln(\frac{\langle dE/dx \rangle}{\langle dE/dx \rangle_X^B}), \tag{3}$$

where $\langle dE/dX \rangle_X^B$ is the expected energy loss based on the Bichsel function and X is the particle type [11]. The raw yield from the TOF are obtained using the variable mass square (m^2), given by

$$m^2 = p^2 \left(\frac{c^2 T^2}{L^2} - 1 \right), \tag{4}$$

where, p, T , L, and c are the momentum, time of travel by the particle, path length and speed of light, respectively. The left panel of Fig 1 shows the average dE/dx of measured charged particles plotted as a function of "rigidity" (i.e., momentum/charge) of the particles. The curves represent the Bichsel expectation values. The right panel of Fig 1 shows the inverse of particle velocity in unit of the speed of light $1/\beta$, as a function of rigidity. The expected values of $1/\beta$ for pions, kaons, and protons are shown as the curves.

In this analysis, for the identification of pion, kaon, and proton, we require TPC $n\sigma$ (z/R; R: TPC resolution)and TOF m^2 cuts which are listed in the Table 1. In addition to m^2 cut a momentum dependent z cut is implemented for light nuclei identification.
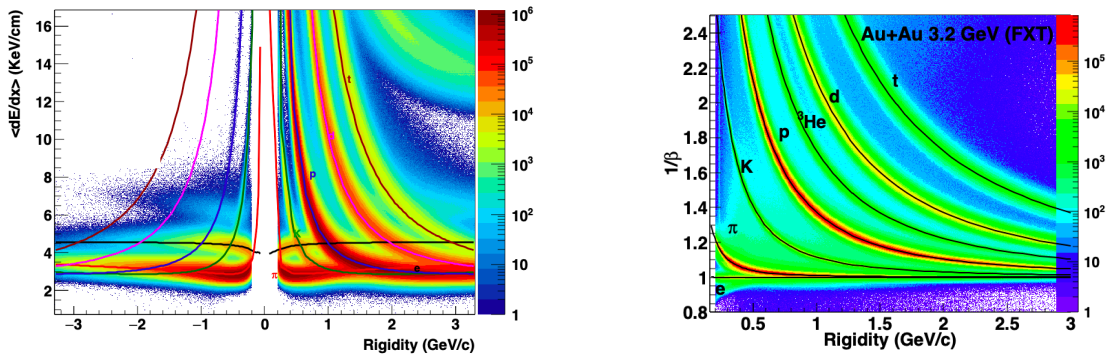
Figure 1: ($\langle dE/dx \rangle$ (left panel) and $1/\beta$ from TOF (right panel) of charged particles in Au+Au collisions at $\sqrt{s_{\mathrm{NN}}} = 3.2$ GeV.

Table 1: $n\sigma$ and m^2 cut for particle identification

pion	$|n\sigma_\pi| < 3$ and $-0.1 < m^2 < 0.15$ $((GeV/c^2)^2)$
kaon	$|n\sigma_K| < 3$ and $0.16 < m^2 < 0.36$ $((GeV/c^2)^2)$
proton	$|n\sigma_p| < 2$ and $-0.6 < m^2 < 1.2$ $((GeV/c^2)^2)$
deuteron	$3.15 < m^2 < 3.88$ $((GeV/c^2)^2)$
triton	$7.01 < m^2 < 8.75$ $((GeV/c^2)^2)$

3.3   Event Plane Reconstruction

The flow coefficients are extracted from the azimuthal angle of particles relative to the azimuth of the reaction plane. However, the reaction plane angle cannot be directly measured in experiments; instead, it can be estimated from the particle azimuthal distribution on an event-by-event basis. This estimated reaction plane is commonly referred to as the event plane. In our calculations, we utilized the first-order event plane angle Ψ_1, which is measured using the Event Plane Detector (EPD). In order to calculate the first-order event plane angle, firstly, we construct the Q vector from particle's azimuthal angle.

$$\vec{Q} = (Q_x, Q_y) = \left(\sum_i w_i \cos(\phi_i), \sum_i w_i \sin(\phi_i) \right), \tag{5}$$

$$\psi_1 = \tan^{-1}(Q_y/Q_x), \tag{6}$$

where sum extends over all detected hits i, and ϕ_i is the azimuthal angle in the laboratory frame, and w_i is the weight for the ith hits, here we use the nMip as the weight, which is the calibrated ADC value. The ψ_1 is the first-order event plane angle [4]. To mitigate acceptance correlations arising from the imperfect detector, it is essential to render the
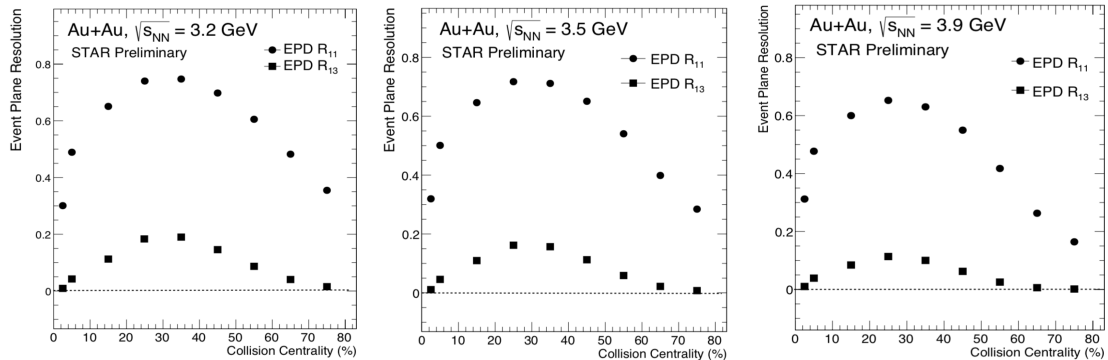
Figure 2: Collision centrality dependence of R_{11} (circles) R_{13} (squares) in Au+Au collisions at $\sqrt{s_{\mathrm{NN}}}=$ 3.2 (left panel), 3.5 (middle panel), and 3.9 GeV(right panel).

event plane angle distribution isotropic or flat. Consequently, a procedure for flattening the event plane angle distribution becomes necessary. In this analysis, we have implemented re-centering and shift corrections to extract a flat event plane angle distribution [4].

3.4 Event Plane Resolution

The finite number of detected particles in detectors produces a limited resolution in the measured event plane angle. So, the observed flow coefficients must be corrected up to what they would be relative to the real reaction plane. This is done by dividing these coefficients by the event plane resolution, estimated from the correlation of the planes of independent subevents.

$$v_n = \frac{v_n^{obs}}{R_n} = \frac{v_n^{obs}}{\langle \cos[n(\psi_n - \Psi_R)]\rangle}, \tag{7}$$

where the R_n is resolution, v_n is the nth harmonic azimuthal anisotropy parameter, and ψ_m is the mth harmonic order event plane, Ψ_r is reaction plane angle. The angle brackets denote an average over all particles in all events [4].

In fixed target mode, the final state particle's acceptance is not symmetric around midrapidity. Therefore, the commonly used 2-sub event method, employed in the collider BES-I analysis, cannot be used to calculate the resolution. This method necessitates each subevent to have similar multiplicity and resolution. Consequently, in this analysis, we opt for the 3-sub event method to calculate the resolution. Figure 2 shows the calculated first-order event plane resolution R_{11} and the third-order event plane resolution R_{13} estimated from the first-order event plane for v_3 calculation, as functions of collision centrality.
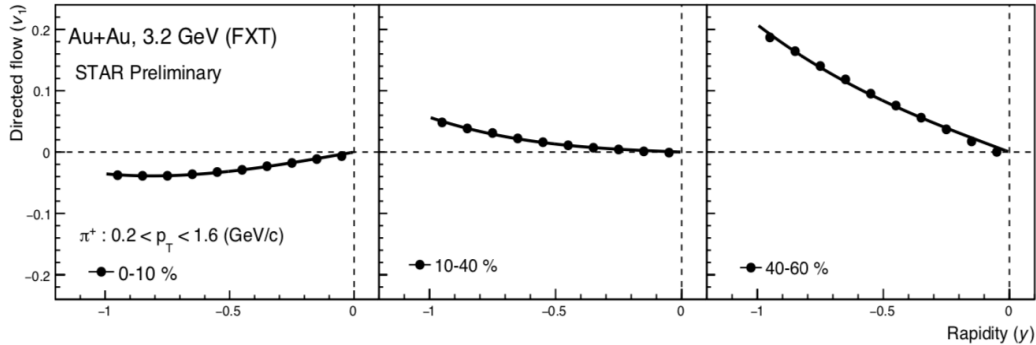
Figure 3: v_1 as a function of y for pion in 0-10% (left panel), 10-40 % (middle panel), and 40-60% (right panel) centrality bin in Au+Au collisions at $\sqrt{s_{\mathrm{NN}}} = 3.2$ GeV. The line represents third order polynomial fit to distribution.

4   Results and Discussion

4.1   Directed Flow (v_1)

The rapidity (y), centrality and collision energy dependence of v_1 for identified hadrons, net-particle, and light nuclei are measured at $\sqrt{s_{\mathrm{NN}}}$= 3.2, 3.5, and 3.9 GeV. Figure 3 illustrates the the centrality dependence of π^+ for $\sqrt{s_{NN}}$= 3.2 GeV. The v_1 changes sign from negative to positive, moving from most central to peripheral collisions, implying the effect of dominant repulsive baryonic interactions and spectator shadowing.

The energy dependence of proton v_1 involves an interplay between the directed flow of protons associated with baryon stopping and particle-antiparticle pair production at mid-rapidity. A means to distinguish between the two mechanisms would thus be to look at the net particle v_1. The net particle represents the excess yield of a particle species over its antiparticle. The net particle's v_1 is defined as

$$v_{1,net} = \frac{v_{1,p} - r v_{1,\bar{p}}}{1 - r}, \tag{8}$$

where $v_{1,p}$, $v_{1,\bar{p}}$ corresponds to particle and anti-particle v_1 and r represents the ratio of anti-particles to particles [9]. Figure 4 shows the y dependence of identified hadrons (left panel), net-particles (middle panel), and light nuclei (right panel) for $10 - 40\%$ centrality. The magnitude of v_1 increases with increasing rapidity for all particles, and a mass ordering is also observed in the magnitude of v_1.

The p_T-integrated $v_1(y)$ slope at mid-rapidity, $dv_1/dy|_{y=0}$, is obtained by fitting the data $v_1(y)$ with a third-order polynomial. Figure 5 shows the collision energy dependence of $dv_1/dy|_{y=0}$ for identified particles (left panel), net-particle (middle panel), and light
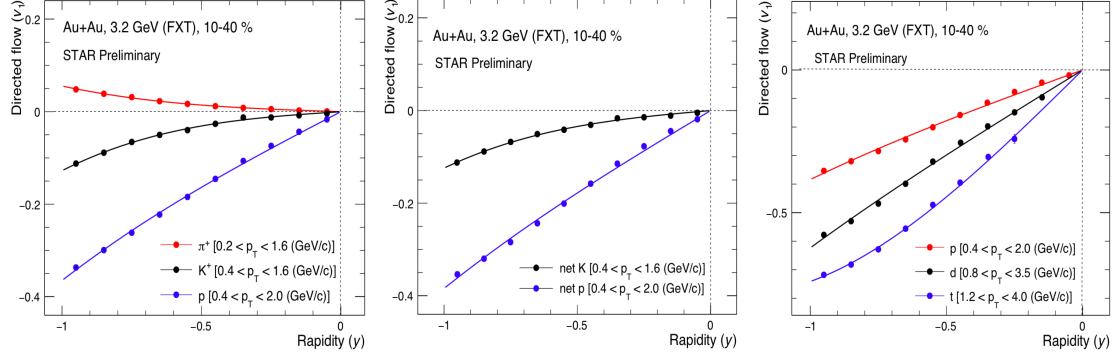
Figure 4: v_1 as a function of y in $10-40\%$ centrality for identified hadrons (left panel), net particles (middle panel) and light nuclei (right panel) in Au+Au collisions at $\sqrt{s_{NN}} = 3.2$ GeV. The line represents 3rd order polynomial fit to distribution.
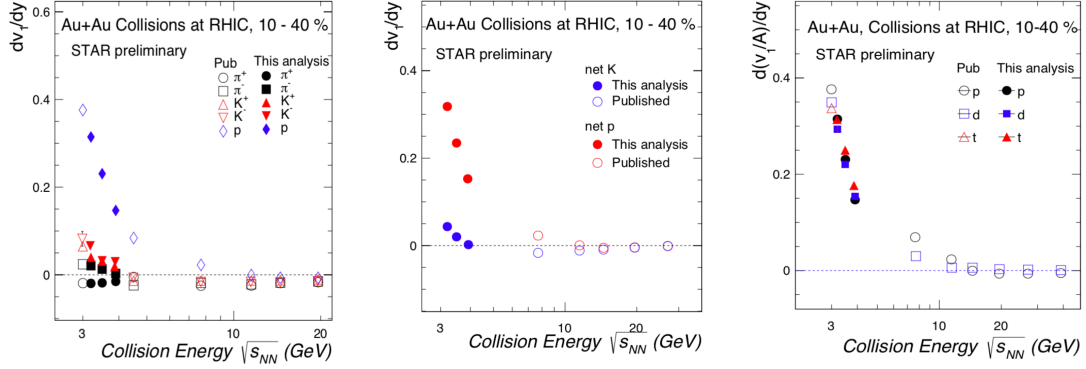
Figure 5: Collision energy dependence of v_1 slope $\mathrm{d}v_1/\mathrm{d}y|_{y=0}$ for identified hadrons (left panel), net particles (middle panel) and light nuclei (right panel) in Au+Au collisions at RHIC for $10-40\%$ centrality. The published data are shown in open markers [12].

nuclei (right panel) in mid-central (10 - 40%) collisions. The extracted slope parameters, $dv_1/dy|_{y=0}$, are scaled by A for light nuclei to compare with protons. The magnitude of the slope decreases with increasing collision energy for all particles, including light nuclei. The slope of v_1 for net-kaon undergoes a sign change from negative to positive at a lower collision energy range ($\sqrt{s_{NN}} = 3.9$ - 7.7 GeV) compared to net-proton ($\sqrt{s_{NN}} = 11.5$ - 19.6 GeV). The light nuclei v_1 slope exhibits an approximate mass number (A) scaling, consistent with the nucleon coalescence mechanism for the production of light nuclei.

4.2 Triangular Flow (v_3)

The y and collision energy dependence of v_3 for identified hadrons and light nuclei are measured at $\sqrt{s_{NN}}=$ 3.2, 3.5, and 3.9 GeV. The left panel of Fig. 6 shows the rapidity dependence of v_3 for identified hadrons. The magnitude of v_3 increases with increasing
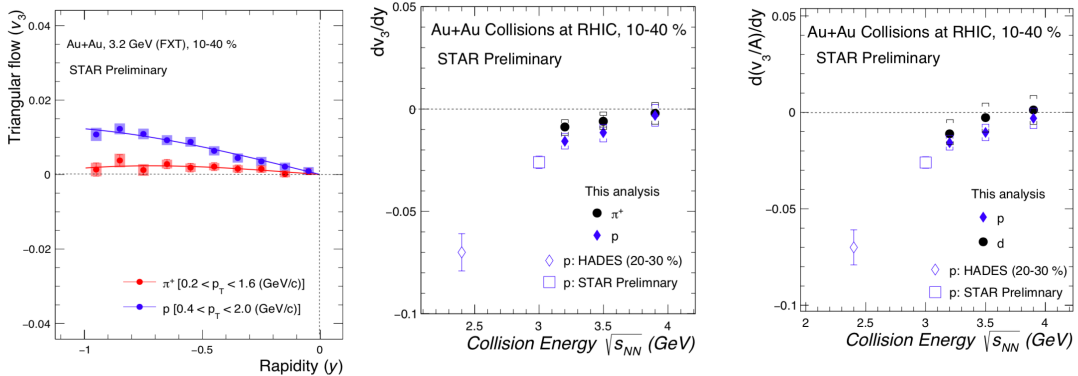
Figure 6: v_3 as a function of y in $10-40\%$ centrality bin for identified hadrons (left panel) in Au+Au collisions at $\sqrt{s_{\mathrm{NN}}} = 3.2$ GeV. Collision energy of $dv_3/dy|_{y=0}$ for identified particles (middle panel) and light nuclei (right panel) in Au+Au collisions at RHIC for $10-40\%$ centrality. The published data are shown in open markers [10].

rapidity. The distribution is fitted with a polynomial of order three to extract the slope parameter.

The middle panel of Fig. 6 shows the slope of v_3, $dv_3/dy|_{y=0}$, for identified hadrons as a function of collision energy. The magnitude of $dv_3/dy|_{y=0}$ decreases with increasing collision energy. It may indicates that the combined effect of the mean-field, baryon stopping, and collision geometry is considerably significant at the low collision energies [13].

The right panel of Fig. 6 shows the extracted slope parameters, $dv_3/dy|_{y=0}$, scaled by mass number (A) for light nuclei. The magnitude of the slope decreases with increasing collision energy. The light nuclei v_3 slope also exhibits an approximate mass number (A) scaling, consistent with the nucleon coalescence mechanism for the light nuclei production.

5   Conclusion

In summary, the rapidity, centrality, and collision energy dependence of directed flow (v_1) of identified hadrons, net particle, and light nuclei in Au+Au collisions at $\sqrt{s_{NN}} = 3.2$, 3.5, and 3.9 GeV is reported. The magnitude of v_1 increases with increasing rapidity for all particles. The extracted v_1 slope of all the particles decreases in magnitude with increasing collision energy. A positive v_1 slope at mid-rapidity for identified hadrons and net particles, excluding π^+, suggests prevalent repulsive baryonic interactions and spectator shadowing. As collision energy decreases, a non-monotonic trend is observed in the slope of both net-kaon and net-proton. The v_1 slope for net-kaon experiences a transition from negative to positive at a collision energy lower than that observed for net-proton. The light nuclei v_1 slope exhibits an approximate mass number scaling consistent with the nucleon coalescence

mechanism for the production of light nuclei. The magnitude of slope of v_3 decreases with increasing collision energy, indicating a substantial collective impact of the mean-field, baryon stopping, and collision geometry at lower collision energies.

References

[1] H. Kastrup, P. Zerwas, eds., QCD - 20 yrs later, World Scientific, Singapore (1993).

[2] A. Aprahamian et. al. DOE/NSF Nuclear Science Advisory Panel (NSAC) Report, (2015).

[3] F.R. Brown, et. al., Phys. Rev. Lett. 65, 2491 (1990).

[4] A. M. Poskanzer and S. A. Voloshin, Phys. Rev. C 58, 1671 (1998).

[5] A. Bialas, M. Gyulassy, Nucl. Phys. B 291, 793 (1987).

[6] B. I. Abelev et al. (STAR Collaboration), Phys. Rev. Lett. 99, 112301 (2007).

[7] H. Liu et al. (E895 Collaboration), Phys. Rev. Lett. 84, 5488 (2000).

[8] P. Danielewicz, R. Lacey, and W. G. Lynch, Science 298, 1592 (2002).

[9] H. Sorge, Phys. Rev. Lett. 78, 2309 (1997).

[10] J. Adamczewski-Musch et al. (HADES), Phys. Rev. Lett. 125, 262301 (2020).

[11] H. Bichsel, Nucl. Instrum. Meth. A 562, 154 (2006).

[12] L. Adamczyk et al. (STAR Collaboration), Phys. Rev. Lett. 120, 062301 (2018).

[13] arXiv: 2309.12610 [nucl-ex] (2023).